Modeling the Solid-State Reaction Between Sn-Pb Solder and a Porous Substrate Coating

K.L. ERICKSON, P.L. HOPKINS, and P.T. VIANCO

Sandia National Laboratories, Albuquerque, NM 87185

Solder joints in hybrid microelectronic circuit electronics are formed between the solder alloy and the noble metal thick film conductor that has been printed and fired onto the ceramic. Although the noble metal conductors provide excellent solderability at the time of manufacture, they are susceptible to solid-state reactions with Sn or other constituents of the solder. The reaction products consist of one or more intermetallic compounds (IMC). The integrity of these solder joints can be jeopardized by formation of IMC layers, which can have thermal and mechanical properties that are substantially different from the solder and substrate and which can consume the conductor layer by solid-state reaction. Analytical models predicting IMC growth for a variety of conditions are needed to improve predictions of long-term joint reliability and manufacturing processes. Unfortunately, because of the inherent porosity of thick film conductors, IMC growth in conductors cannot be well predicted by simply applying growth kinetics to a quasi-one-dimensional layer geometry. Rather, IMC growth involves a complicated geometry in which the interfaces between solid-state phases grow, intersect, and coalesce. In such geometries, explicit boundary tracking, which is normally done in one-dimensional models, is impractical. In heat transfer analyses, an implicit approach, referred to as the enthalpy method, has been used to address multidimensional problems in which interface displacement is controlled by an energy flux. However, an analogous general approach has not been available for mass transfer and reaction analyses. This paper discusses initial 2-D results from a coupled experimental and computational effort to develop a mathematical model and computer code that will ultimately predict 3-D intermetallic growth in porous substrate-solder systems. The numerical model is based on an implicit interface tracking approach developed for diffusion-reaction analyses in complicated geometries. To illustrate the implicit approach with a "real" system, the 2-D calculations were based on the reaction couple formed between 63Sn-37Pb solder and 76Au-21Pt-3Pd substrates. Physical constants in the model were evaluated from experimental data. Consumption of the thick film was predicted as a function of time and compared with data from independent experiments.

Key words: Diffusion-reaction modeling, intermetallic compound, intermetallic growth, porous substrate, solder, solid-state reaction

INTRODUCTION

Solder joints in hybrid microelectronic circuit (HMC) electronics are formed between the solder alloy and the thick film conductor that has been printed and fired onto the ceramic. Although the noble metal conductors provide excellent solderability at the time of manufacture, they are susceptible to solid-state reactions with Sn or other constituents of the solder. The reaction products consist of one or more intermetallic compounds (IMC). The integrity of these solder joints can be jeopardized by formation of IMC layers, which can have thermal and mechanical properties that are substantially different from the solder and substrate and which can consume the conductor layer by solid-state reaction. Analytical models predicting IMC growth for a variety of conditions are needed to improve predictions of long-term joint reliability and manufacturing processes.

Unfortunately, because thick film conductors are inherently porous, IMC growth cannot be well predicted by applying growth kinetics to a quasi-one-

(Received March 4, 1998; accepted June 19, 1998)

dimensional geometry. The porosity of the films is significant, about 36 percent in the samples discussed below, and during processing, molten solder penetrates a substantial portion of the pore space. The resulting boundary between solder and base metal generally will have a complicated 3-D geometry. As subsequent intermetallic growth occurs, the solder in the pores and the surrounding base metal are consumed, and IMC growth involves a complicated geometry in which the boundaries between solid-state phases grow, intersect, and coalesce. Analysis of IMC growth in porous conductors is, therefore, much more challenging, both experimentally and computationally, than analysis of one-dimensional growth in nonporous materials. Experimentally, IMC growth mechanisms and kinetics must be determined regardless of geometry. However, in the case of porous conductors, characterization of the pore space and solder penetration also must be considered. Computationally, explicit boundary tracking, which is normally done in one-dimensional models, is impractical due to the complicated geometry in which the boundaries between solid-state phases grow, intersect, and coalesce. In heat transfer analyses, an implicit approach, referred to as the enthalpy method,[1] has been used to address multidimensional problems in which boundary displacement is controlled by an energy flux. Some cases involving solute transport also have been addressed with enthalpy-type methods. Crowley and Ockendon[2] used such an approach to model solidification of a dilute alloy. Unfortunately, an analogous general approach has not been available for mass transfer and reaction analyses. However, other implicit techniques have been applied to solute transport. For example, Warren and Boettinger[3] used the "phase-field" approach to model solidification of a binary alloy. Also, an interesting analysis of the departure from local equilibrium at the interface of a binary diffusion couple was given by Langer and Sekerka.[4]

This paper discusses initial 2-D results from a coupled experimental and computational effort to develop a mathematical model and computer code that will ultimately predict 3-D intermetallic growth in porous substrate-solder systems. The numerical model is based on an implicit boundary tracking approach developed for diffusion-reaction analyses in complicated geometries. To illustrate the implicit approach with a "real" system, the 2-D calculations were based on the reaction couple formed between 63Sn-37Pb solder (wt. percent) and 76Au-21Pt-3Pd (wt. percent) substrates. The major assumptions in the calculations were that: (1) IMC layer growth could be considered diffusion controlled; (2) for the purpose of illustrating the implicit approach, layer growth could be modeled in terms of a pseudo-binary system consisting of $Au_{0.74}Pt_{0.21}Pd_{0.05}$ and Sn, and (3) volume changes due to chemical reaction could be neglected. Physical constants in the model were evaluated from experimental data. In particular, during previous work,[5] IMC growth as a function of time was studied in isothermal aging experiments involving 63Sn-37Pb solder and 76Au-21Pt-3Pd alloy sheet and porous thick films. The data from the alloy sheet experiments provided growth rate data for a simple one-dimensional geometry that facilitated analysis of kinetics and parameter evaluation. The porous thick film experiments provided independent data for comparison with numerically predicted film consumption. Preliminary characterization of the pore structure was done by image analysis of micrographs obtained by scanning electron microscopy (SEM) in the backscattered electron (BSE) mode.

In the text below, the sequence of discussion is the following. First, the experimental techniques and results for the experiments with 63Sn-37Pb solder and 76Au-21Pt-3Pd alloy sheet and thick films are briefly summarized, including pore structure characterization of the thick films. Next, the equations governing IMC growth in terms of explicit boundary tracking are reviewed. The implicit approach used in this work is then described; after which, numerical implementation of the model is briefly discussed, and initial 2-D numerical results based on the experimentally determined parameter values and pore space characterization are given. Consumption of the thick film, predicted as a function of time, is compared with data from thick film isothermal aging experiments. Finally, some conclusions and recommendations for further work are offered.

EXPERIMENT

IMC Growth

To examine IMC growth mechanisms and kinetics, isothermal aging experiments were done using 63Sn-37Pb solder and 76Au-21Pt-3Pd alloy sheet, which provided a one-dimensional geometry that facilitated examining growth mechanisms without complicated geometrical effects that occur in the porous thick film conductor. Alloy sheet having a composition of 76Au-21Pt-3Pd (wt. percent) was obtained from a commercial fabricator. Chemical certification of the stock composition was provided by the manufacturer; no additional assays were performed. The sheet was cut into tabs $6.4 \times 6.4 \times$ 0.38 mm. The tabs were used in the as-rolled and cut condition, since the characteristic dimensions of the surface roughness on the tabs were much smaller than the anticipated IMC layer thicknesses. Each tab was immersed in a bath of 63Sn-37Pb solder (212 ±2°C) for 15 s and then withdrawn, leaving one broad face parallel to the bath surface. Using this technique, a large quantity of solder remained attached to the surface, thereby making certain that a near-infinite supply of solder was available for IMC layer growth.

The aging temperatures were 55, 70, 85, 100, 135, and 170°C. The aging times ranged from 5 to 5000 h. The isothermal heat treatments were performed in air furnaces with temperature control of ±1°C; the aging time was held to within ±5 min for total periods of less than 250 h and within ±30 min for longer

Table I. IMC Growth with 63Sn-37Pb Solder and 76Au-21Pt-3Pd Alloy Sheet

Temp. (°C)	Time (h)	Pseudo-$AuSn_4$ Layer (μm)		Pseudo $AuSn_2$ Layer (μm)	
		Mean	Std. Dev.	Mean	Std. Dev.
85	20	0.45	0.1	0.0	0.0
	50	0.36	0.1	0.0	0.0
	250	0.21	0.03	0.0	0.0
	1000	0.55	0.11	0.0	0.0
	2000	0.81	0.19	0.0	0.0
	5000	1.82	0.73	0.0	0.0
				0.0	0.0
100	20	0.13	0.16	0.0	0.0
	50	0.57	0.15	0.0	0.0
	250	0.72	0.18	0.0	0.0
	1000	1.05	0.28	0.0	0.0
	2000	5.68	0.88	0.0	0.0
	5000	4.21	1.47	7.31	1.57
				0.0	0.0
135	5	0.86	0.14	0.0	0.0
	20	3.13	0.84	0.0	0.0
	50	13.34	2.67	0.0	0.0
	250	22.8	2.1	25.41	—
	1000	103.4	8.7	0.0	0.0
				0.0	0.0
170	5	9.61	2.81	0.0	0.0
	20	40.85	2.71	0.0	0.0
	1000	344.8	17.8	0.0	0.0

durations. The intermetallic compound layer thickness measurements were made on 1000x SEM/BSE photomicrographs showing cross-sectional views of the interface between the solder and the bulk metal. A total of six such locations were photographed per sample. Ten thickness measurements were made along the interface, at 13 μm intervals. A total of 60 thickness measurements were made per aging treatment condition. The data were described by the mean thickness value and a scatter term representing ±1 standard deviation. In those instances in which two sublayers were visible at the interface, the total thickness was measured along with that of the sublayer closest to the Au-Pt-Pd metal; the second sublayer thickness was determined by subtracting the first sublayer thickness from the total thickness value at each location. Representative results are shown in Table I and indicate that generally only one intermetallic layer formed.

Growth of that layer appears to involve multiple mechanisms, as indicated in Fig. 1, which shows layer growth vs $\sqrt{t}$ for temperatures of 100, 135, and 170°C. Layer growth is relatively slow during an initial induction period, after which growth is much more rapid. The induction period decreases with temperature. At 135°C, the major portion of the layer growth appears linear with $\sqrt{t}$, which was assumed to be indicative of a diffusion controlled regime, and at 170°C, layer growth appears essentially linear with $\sqrt{t}$, although data are limited. Furthermore, the elemental composition of the IMC layer was found to be approximately $Au_{0.74}Pt_{0.21}Pd_{0.05}Sn_4$ so that growth of the layer could be modeled in terms of a pseudo-binary system consisting of $Au_{0.74}Pt_{0.21}Pd_{0.05}$ and Sn.

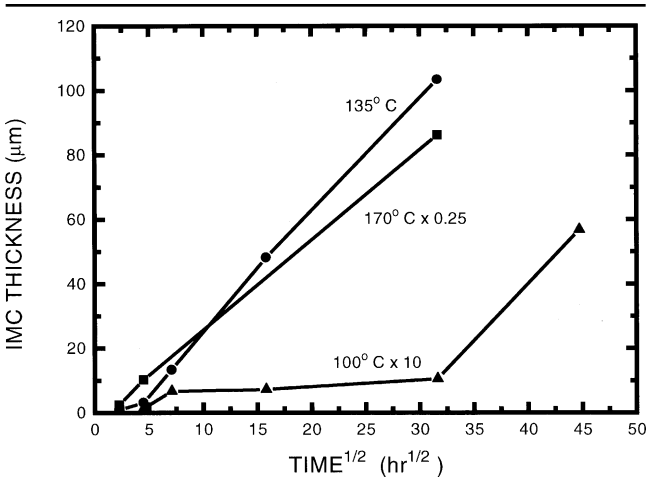

Fig. 1. Experimental data for IMC growth vs $\sqrt{t}$ for temperatures of 100, 135, and 170°C.

Isothermal aging experiments with 63Sn-37Pb solder and 76Au-21Pt-3Pd thick film samples were done to provide data for intermetallic compound growth that could be compared with numerically predicted film consumption. The thick film composition was screen printed on 96 percent alumina substrate with a pattern of a series of 1.0×1.0 mm square pads. A double printing process was used in which the first ink deposit was screen printed onto the alumina substrate; the deposits were allowed to dry under conditions of 150°C and 10 to 15 min exposure in dry nitrogen. The substrate was then fired at 825°C for 10 min. Then, the second printing of ink was applied to the substrate; the ink was dried, and the substrate fired again at 825°C for 10 min. Solder alloy 63Sn-

37Pb was applied to each of the pads by screen printing a paste that also contained a rosin-based, mildly activated flux. The solder was reflowed by the vapor phase technique; the processing conditions were 212°C for 30 s. Each test sample (coupon) had three such solder bumps.

One test coupon was heat treated at each of the set aging conditions. The aging temperatures were 55, 70, 85, 100, 135, and 170°C. The aging times ranged from 1 to 18,104 h (2.06 years). The isothermal test coupons were metallographically cross sectioned through each of the three solder bumps, mounted in cold-setting epoxy, and polished. Viewing of the interface was performed using SEM in the BSE mode. A total of ten intermetallic compound layer thickness values were taken on each of the three solder bumps. Details of the procedure used to perform the measurements were described previously.[5] At the location from which each intermetallic compound layer measurement was obtained, the residual thick film thickness was also measured.

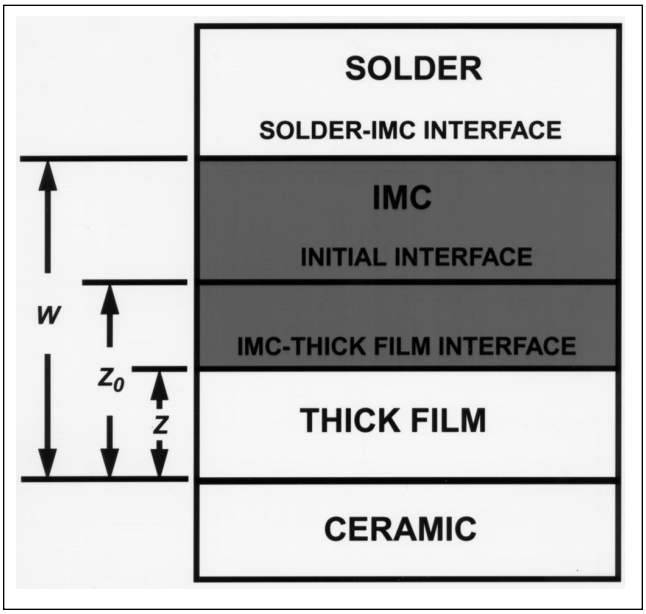

Fig 2. Schematic diagram illustrating solder-IMC and IMC-thick film interface displacement relative to the original solder-thick film interface.

The displacements of the solder-IMC interface and the IMC-thick film interface, relative to the solder-thick film interface prior to aging, were determined as follows. Referring to Fig. 2 and neglecting volume changes due to chemical reaction, the displacement of the IMC-thick film interface was calculated by subtracting the thick film thickness (z) remaining after aging from the original thickness (z_0). The displacement of the solder-IMC interface was calculated by first adding the remaining thick film thickness (z) to the intermetallic compound layer thickness (w-z) which gave the current position (w) of the interface. Then the original thick film thickness (z_0) was subtracted from w to give the relative displacement of that interface after the start of solid state aging. Representative results are given in Table II.

Table II. IMC Growth with 63Sn-37Pb Solder and 76Au-21Pt-3Pd Thick Film

Temp. (°C)	Time (h)	IMC ($AuSn_4$) Layer Thickness (μm)		Mean Boundary Displacement Relative to the Initial Interface (μm)	
		Mean	Std. Dev.	Solder-IMC	IMC-Thick Film
100	0	1.05	0.21		
	20.3	1.12	0.32		
	51.7	1.18	0.47		
	100	1.64	0.37		
	216.5	1.90	0.36		
	400	2.99	0.56		
	751	2.31	0.32	1.58	0.73
	1009	3.18	0.41	1.76	1.42
	1487	3.78	0.55		
	2004	5.79	0.68	3.97	1.82
	5002	13.3	1.8	9.33	4.0
	18104	44.6	8.0	31.4	13.2
135	0	1.05	0.21	—	—
	61	6.08	0.90	4.88	1.20
	120	8.96	1.23	—	—
	182.3	19.6	2.89	16.0	3.6
	273.8	21.5	3.18	17.0	4.5
170	0	1.05	0.21	—	—
	5	9.92	2.07	8.72	1.2
	25	40.5	6.25	34.9	5.8
	53	66.6	10.1	48.9	17.7
	102	71.7	7.98	51.7	20.0

Pore Space Characterization

Four SEM/BSE micrographs (1000x) were taken of the 76Au-21Pt-3Pd thick film conductor that had formed a couple with 63Sn-37Pb solder. One such micrograph is shown in Fig. 3. The alumina substrate is at the bottom of the micrograph and appears as solid black. The porous thick film on the ceramic appears as the light gray layer containing dispersed black regions, which are voids. The solder above the thick film appears as the dark gray layer (Sn-rich phase) containing dispersed light gray regions (Pb-rich phase). A very thin layer of the IMC is visible at the interface of the solder and thick film. The thick film coating area that was viewed was approximately 19 μm by 111 μ m. The images of the thick film layer were then digitized. The extent of porosity, which included the total number of pores, mean and standard deviation of the pore area, and discrete pore area distribution were determined using quantitative image analysis software. The unfilled pore size distribution and the total pore size distribution (unfilled pores plus pores filled with solder) were assessed. The total porosity (pores both filled and not filled with solder) was 36 percent, and the unfilled porosity was 26 percent. Furthermore, similar analyses of sections made parallel to the plane of the thick film at different depths gave similar results and indicated that the pore structure was approximately uniform throughout the thick film.The more detailed pore measurements for this sample are summarized in Table III. However, current information on the extent of initial solder penetration into the pores of the thick films is limited. Initial analyses indicated that about 68 percent of the available pores at the surface contained solder to an average depth of about 8.8 μm below the initial solder-thick film interface.

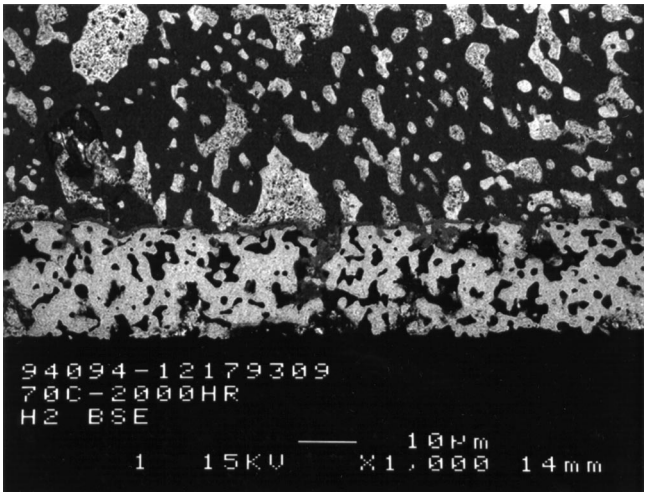

Fig. 3. SEM/BSE micrograph (1000x) showing porous 76Au-21Pt-3Pd film conductor (lower) and solder (upper) regions.

Table III. Two-Dimensional Thick Film Pore Structure Characterization

Region of interest area	2.625×10^{-3} mm^2
Number of pores	220
Total pore area	6.864×10^{-4} mm^2
Minimum pore area	1.267×10^{-7} mm^2
Maximum pore area	5.054×10^{-5} mm^2
Mean pore area	3.112×10^{-6} mm^2
Total Porosity	36%

THEORY

The usual approach for modeling intermetallic layer growth is to assume that the individual layers are separated by ideal planar interfaces, the intermetallic compounds on either side of which are distinctly different. The conversion of the intermetallic compound on one side of the interface to that on the other side occurs at the interface, and the movement of the interface between layers is modeled explicitly as described in more detail below. In reality, each intermetallic layer is separated from an adjacent layer by a thin reaction zone, of at least atomic dimensions, in which the intermetallic compound of one layer is continuously converted to that of the adjacent layer. The assumption of a planar interface is an idealization that has been used very successfully in one-dimensional analyses and has been particularly useful for obtaining analytical solutions. Unfortunately, the approach is not easily implemented in multidimensional problems involving complicated geometries with multiple intersecting and coalescing interfaces. In heat transfer analyses involving phase transitions, this problem is circumvented by using the enthalpy method, which determines the movement of phase boundaries, or interfaces, implicitly, but which does not have a general analogy in mass transfer.

To model intermetallic layer growth in such complicated geometries, an implicit approach has been developed in which the ideal interface is replaced by a thin reaction zone in which the intermetallic compound of one layer reacts rapidly to form the compound of the adjacent layer. The reaction rate expressions are included in the diffusion equations for the diffusing constituents so that the explicit equations for displacement of the interfaces are eliminated, and interface displacement is determined implicitly by the reaction of one compound to another. A more detailed description of this implicit approach is given below after first summarizing the usual explicit approach. To facilitate illustrating the basic ideas in the implicit approach, the governing equations for the explicit and implicit approaches are illustrated for one-dimensional layer growth, after which the extension of the implicit equations to three dimensions immediately follows.

Explicit Interface Displacement

During previous work, the literature pertaining to the governing equations based on explicit interface displacement for modeling intermetallic growth was reviewed, and a general model describing one-dimensional growth of multiple intermetallic layers was developed and implemented in a one-dimensional

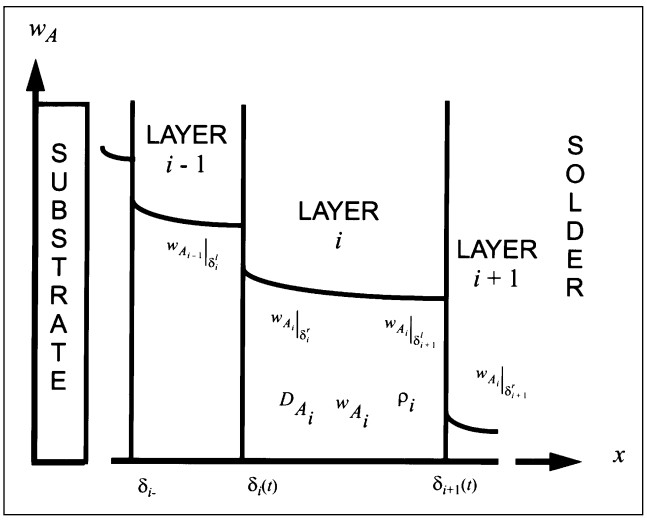

Fig. 4. Schematic diagram showing intermetallic layer growth between substrate and solder.

computer code based on the method of lines. A summary of that literature review, the resulting model in which displacements of the interfaces between layers were calculated explicitly, and the corresponding code development, as well as application of the code (ILaG) to the analysis of experimental data from the 100Sn/Cu and 63Sn-37Pb/Cu systems were reported in earlier publications.[6,7] That work provided a basic model and computer code with which an implicit approach could be developed for a variety of IMC growth mechanisms and verified for a one-dimensional geometry.

The explicit model consists of a set of material balance equations for each layer and displacement equations for the interfaces on each side of the layer. The material balance equations describe bulk diffusion of the rate-controlling constituent in each layer. The model was developed to accommodate cases involving:

- Finite initial layer thicknesses,
- Rate-limiting interfacial reactions,
- Multiple and variable diffusion coefficients, and
- Finite material boundaries.

Additionally, the effects of nucleation could be modeled empirically. Results from the one-dimensional code were verified by comparing the numerical results with analytical solutions for simple systems involving two, three, and five layers, and constant valued physical properties. In more recent work, the model and code were extended for the analysis of nonisothermal intermetallic layer growth. Temperature-dependent diffusion coefficients and interfacial reaction rate constants were represented by Arrhenius expressions.[8] A brief description of the resulting model is presented below and provides a frame of reference for discussing the implicit approach.

Consider a substrate-solder system in which I-l intermetallic layers form and grow between the substrate and bulk solder as shown schematically in Fig. 4. Let the substrate form the left boundary of the system, and the solder the right boundary. Let i = 1,2,3,...,I-1 denote the sequence of intermetallic layers growing from left to right. That is, i = 1 denotes the layer adjacent to the right edge of the substrate (layer 0), and i = I-1 denotes the layer adjacent to the left edge of the solder (layer I). Growth of the intermetallic layers results from interfacial reaction and diffusion of a binary set of interacting constituents. In each layer, the diffusion of either constituent can be rate controlling.

For this work, diffusion was assumed to occur primarily through the bulk IMC layers since insufficient data was available to differentiate between bulk and grain boundary diffusion. Terms for bulk motion of the IMC lattice were not included in the material balances since insufficient information was available to examine Kirkendall effects. Within an IMC layer, equilibrium between the bulk IMC and the diffusing constituents was assumed so that net formation of the IMC occurred only at the interfaces between layers. Finally, volume changes due to chemical reaction and compositional variation were neglected since those effects are often small. For example, the volume change occurring in the reaction $Au + 4Sn \rightarrow AuSn_4$ is about 3 percent of the volume of the $AuSn_4$ formed. While this is a substantial change with respect to inducing stress and strain, it is a small change with respect to interface displacement.

Let T denote temperature; t denote time; x denote position with respect to a fixed origin; $\delta_i(t)$ the position of the interface between layer i-1 and layer i, and $\Delta_i(t)$ the thickness of layer i

$$\Delta_i(t) = \delta_{i+1}(t) - \delta_i(t) \tag{1}$$

Then, for $\delta_i(t) < x < \delta_{i+1}(t)$, the material balance for the rate controlling constituent in each layer is given by

$$\frac{\partial}{\partial t}\left(\rho_i W_{A_i}\right) = \frac{\partial}{\partial x}\left(\rho_i D_{A_i} \frac{\partial W_{A_i}}{\partial x}\right) \tag{2}$$

where W_{a_i} denotes the mass fraction of the rate-controlling constituent in layer i; ρ_i denotes the mass density of layer i, and D_{A_i} denotes the diffusion coefficient, which can be a function of x, t, W_{a_i}, and T, and can be specified accordingly. For frequent cases of interest, D_{A_i} is given by an Arrhenius expression

$$D_{A_i} = D_{A_{i_0}} \exp\left(-Q_{A_i} / RT\right) \tag{3}$$

where $D_{A_{i_0}}$ is a constant; Q_{A_i} is the activation energy for diffusion of the constituent in layer i, and R is the gas constant. In general, the temperature T can be a function of x and t, which also can be specified.

When constituent diffusion and interface displacement are not hindered by finite material boundaries, and the rate of interfacial chemical reaction is sufficiently fast, local chemical equilibrium exists at the interface, and the concentrations of the diffusing constituents in layer i are essentially constant at $\delta_i(t)$ and $\delta_{i+1}(t)$. Therefore, at $\delta_i(t)$, the boundary condition for Eq. (2) is

$$W_{A_i}\Big|_{\delta_i^r} = \text{constant} \tag{4}$$

and at $\delta_{i+1}(t)$, the boundary condition is

$$W_{A_i}\Big|_{\delta_{i+1}^{l}} = \text{constant} \tag{5}$$

where $W_{A_i}\Big|_{\delta_i^r} \neq W_{A_i}\Big|_{\delta_{i+1}^{l}}$,

and superscripts l and r denote values at the left and right sides of the interface, respectively. Equations (4) and (5) reflect the maximum and minimum concentrations, respectively, of constituent A that occur in the intermetallic compound. The maximum and minimum concentrations of A are determined by the defect equilibria for the IMC. For substitutional defects, the maximum and minimum concentrations for many IMCs can be obtained from the respective phase diagrams. The initial condition for Eq. (2) is

$$W_{A_i}(x,0) = f_i(x) \tag{6}$$

where $f_i(x)$ is known or assumed.

When the rate of interfacial reaction is slow enough to preclude local equilibrium at the interface, the constant concentration boundary conditions given by Eq. (4) and Eq. (5) must be replaced by more complicated boundary conditions involving expressions for the diffusion fluxes and rates of interfacial reaction of constituent A at the interface $\delta_i(t)$. Furthermore, when constituent diffusion encounters a finite material boundary, the boundary condition for Eq. (2) is that the constituent flux vanishes at that boundary.

The displacement of each interface is given explicitly by

$$\left[\rho_{i-1} W_{A_{i-1}}\Big|_{\delta_i^l} - \rho_i W_{A_i}\Big|_{\delta_i^r}\right]\frac{d\delta_i}{dt} = \tag{7}$$

$$-\rho_{i-1} D_{A_{i-1}} \frac{\partial W_{A_{i-1}}}{\partial x}\Big|_{\delta_i^l} + \rho_i D_{A_i} \frac{\partial W_{A_i}}{\partial x}\Big|_{\delta_i^r}$$

and the initial condition for Eq. (7) is

$$\delta_i(t=0) = \delta_i^0 = \text{a constant} \tag{8}$$

Implicit Interface Displacement

While the system of equations described above can be solved efficiently, the explicit nature of the interface tracking makes the extension to multiple dimensions extremely difficult, particularly with regard to numerical methods, for complex geometries. However, an implicit approach appears feasible in which the ideal interface is replaced by a thin reaction zone in which the material of one layer undergoes a rapid, quasi-homogeneous reaction to form the compound of the adjacent layer. From a physical perspective, such an approach has considerable appeal since it mimics actual phenomena, but from a practical perspective, some annoying difficulties exist. In particular, the mechanisms and kinetics for the solid-state interfacial reactions of many materials of interest are unknown. Furthermore, in the reaction zone approach, a homogeneous analogy must be used to approximate a heterogeneous interfacial reaction. Fortunately, the rates of those reactions are often rapid relative to the rate of solid-state diffusion of the reacting constituents, so that local equilibrium exists with respect to an ideal interface, which is the boundary condition expressed previously by Eq. (4) and Eq. (5). For initial model development, the local equilibrium condition is more convenient to work with than the more general case involving rate-limiting interfacial reactions. Therefore, the discussion below is limited to cases in which local equilibrium exists at the interfaces between phases, and for purposes of initial calculations, only one reaction product layer is considered.

In the case of local equilibrium, any reasonable set of reactions can be used to represent the reaction zone provided that the reactions are sufficiently rapid so that the width of the reaction zone remains within prescribed limits, and the stoichiometries of the products in the reaction zone remain consistent with those given by the phase diagram for the reacting materials. This can be more fully explained by considering the following example.

Consider a substrate material A and solder B which react to form the intermetallic compound AB_m, as shown schematically in Fig. 5. The reaction zone between materials A and AB_m consists of material in both the A lattice and product AB_m lattice, through which A diffuses away from, and B diffuses to the A lattice. The homogeneous analogy to the interfacial reaction must account for B displacing material A from the A lattice and then combining with material A remaining in the A lattice to form AB_m, which is then incorporated into the AB_m lattice. Most of material A is immobile and occupies sites in the A or AB_m lattices. However, at any time, a small fraction of material A is essentially mobile as a result of interaction with the defects in equilibrium with the lattice sites. In the previous explicit approach, no advantage would have been gained by distinguishing between mobile and immobile material A. However, formulating the equations for the implicit approach is facilitated by assuming that material A consists of an immobile species $\overline{A}$ and a mobile species A. The immobile species $\overline{A}$ is part of the A lattice until $\overline{A}$ reacts with B to form AB_m

$$\overline{A} + mB \rightarrow AB_m \tag{9}$$

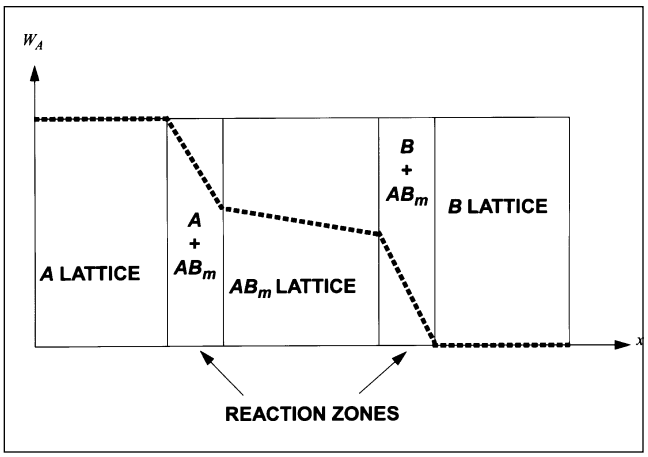

Fig. 5. Schematic diagram showing thin reaction zone approximation for implicit interface tracking method.

The product AB_m is immobile and becomes part of the AB_m lattice. The rate of reaction is given by an expression of the form

$$r_{AB_m} = f\left(w_{\overline{A}}, w_B\right) \tag{10}$$

where r_{AB_m} is the molar rate of production of AB_m per unit volume, and the terms $w_{\overline{A}}$ and w_B are the mass fractions of $\overline{A}$ and B, respectively. The mobile species A is the material that is displaced from the A lattice, as a result of defect interactions during the formation of AB_m, and then diffuses through the AB_m lattice. The displacement of material from the A lattice is represented by the reaction

$$\overline{A} \rightarrow A \tag{11}$$

and the rate of formation of A, denoted by r_A, is proportional to r_{AB_m} above.

To provide for the necessary concentration gradient in mobile A across the AB_m layer, the simplest, though least physically appealing, approach is to let material A initially have a small, uniformly distributed mass fraction of A, such that

$$w_A(t=0) = w_{A_{max}} - w_{A_{min}} \tag{12}$$

where $w_{A_{max}}$ and $w_{A_{min}}$ are the maximum and minimum values, respectively, for the mass fraction of constituent A in the product AB_m and are the same values that were discussed in conjunction with Eq. (4) and Eq. (5).

In the reaction zone between the AB_m and B lattices, a similar quasi-homogeneous analogy to the interfacial reaction is based on an immobile species $\overline{B}$ and mobile species B, so that as A diffuses into the reaction zone

$$A + m\overline{B} \rightarrow AB_m \tag{13}$$

and

$$\overline{B} \rightarrow B \tag{14}$$

where $r_{AB_m} = f(w_A, w_{\overline{B}})$, and $r_B \sim r_{AB_m}$. Similarly, to provide for the necessary concentration gradient of B across the AB_m layer,

$$w_B(t=0) = w_{B_{max}} - w_{B_{min}} \tag{15}$$

where $w_{B_{max}} = 1 - w_{A_{min}}$ and $w_{B_{min}} = 1 - w_{A_{max}}$.

The thin reaction zone approximation described above is the basis for implicit interface tracking. This approach involves two mobile species A and B as well as three immobile species, the reaction product AB_m and the two pseudo species $\overline{A}$ and $\overline{B}$. The governing equations for this approach consist of the following material balances for each species. The material balance for mobile A is given by

$$\frac{\partial}{\partial t}\left(\rho w_A\right) = \frac{\partial}{\partial x}\left(D_A \frac{\partial}{\partial x}\left(\rho w_A\right)\right) + M_A \overline{R} \tag{16}$$

or more generally

$$\frac{\partial}{\partial t}\left(\rho w_A\right) = \nabla \bullet \left[D_A \nabla\left(\rho w_A\right)\right] + M_A \overline{R} \tag{17}$$

where subscripts denoting layer i have been omitted; w_A is the mass fraction of the diffusion-controlling species A; ρ is the material mass density; M_A is the molecular weight of species A, and D_A is the effective diffusion coefficient. The term $\overline{R}$ represents the sum of the terms for the rates of production and depletion of species A and is given by

$$\overline{R} = \sum_{j=1}^{2} m_j r_j \tag{18}$$

where the reaction rates r_j and coefficients m_j are discussed in more detail below.

The reaction rate given by r_1 is the rate of depletion of A due to the reaction given by Eq. (13), and the reaction rate r_2 is the rate of production of A due to the reaction given by Eq. (11). Reaction rates were assumed to be first order in the layer forming constituents

$$r_1 = \frac{\rho^2}{M_A M_B} \underline{k_1} w_A w_{\overline{B}} \tag{19}$$

$$r_2 = \frac{\rho^2}{M_A M_B} \overline{k}_{\overline{1}} w_{\overline{A}} w_B \tag{20}$$

where $\underline{k_1}$ and $\overline{k}_{\overline{1}}$ denote reaction rate constants chosen sufficiently large relative to the value of D_A, so that the reaction zone is thin relative to the IMC layer thicknesses of interest. The coefficient m_j and Eq. (18) are given by

$$m_1 = -1 \tag{21}$$

$$m_2 = \frac{M_{AB_m} - M_A}{M_A} \tag{22}$$

The time rate of change of species AB_m is given by

$$\frac{d}{dt}\left(\frac{\rho w_{AB_m}}{M_{AB_m}}\right) = r_1 + r_2 \tag{23}$$

where r_1 is the rate of production of AB_m due to the reaction given by Eq. (13), and r_2 is the rate of production due to Eq. (9). The time rate of change of species $\overline{A}$ is given by

$$\frac{d}{dt}\left(\frac{\rho w_{\overline{A}}}{M_{\overline{A}}}\right) = -\left[1 + \frac{M_{AB_m} - M_A}{M_A}\right] r_2 \tag{24}$$

where the term involving r_2 is the rate of depletion of $\overline{A}$ due to the reactions given by Eq. (9) and (11). The time rate of change of species $\overline{B}$ is given by

$$\frac{d}{dt}\left(\frac{\rho w_{\overline{B}}}{M_{\overline{B}}}\right) = -\left[m + \frac{M_{AB_m} - M_B}{M_B}\right] r_1 \tag{25}$$

where the term involving r_1 is the rate of depletion of $\overline{B}$ due to the reactions given by Eq. (13) and Eq. (14).

The mass fraction of species B is obtained from the requirement that the mass fractions of all species sum to one

$$w_B = 1 - w_A - w_{AB_m} - w_{\overline{A}} - w_{\overline{B}} \quad (26)$$

The total mass fraction of species A is given by

$$W_A = w_A + \left(\frac{M_A}{M_A + mM_B}\right) w_{AB_m} + w_{\overline{A}} \quad (27)$$

and the mass density by

$$\rho = \frac{\rho_A \rho_B}{\rho_A + (\rho_B - \rho_A) W_A} \quad (28)$$

To initially verify the implicit approach described above, a one-dimensional test problem was solved using both explicit, Eqs. (2), (4)–(6), and (7) and (8), and implicit, Eqs. (16) and (18)–(28), formulations. Interface displacement was computed explicitly using the previously mentioned method of lines code ILaG. Interface displacement was computed implicitly by implementing Eqs. (16) and (18)–(28) in the finite element, multidimensional heat conduction code COYOTE II, as discussed in Appendix A. The test problem consisted of the binary system of species A and B reacting to form one intermetallic layer, AB, as A and B inter-diffuse. Initially, a small (1 micron) layer of AB exists at x = 0, with A to the left (x < 0) and B to the right (x > 1 micron). Typical values for the diffusion coefficient and other parameters were selected from previous work.[6,7] Profiles for the total mass fraction of A, denoted by W_A, at three different times are compared in Fig. 6 for both explicit (ILaG) and implicit (COYOTE) approaches. Although this test problem was relatively simple, analogous one-dimensional test problems can, in principle, be used to verify the implicit approach for much more complicated systems since ILaG provides a capability to explicitly compute interface displacement for a variety of systems involving rate-limiting interfacial reactions, multiple and variable diffusion coefficients, finite material boundaries, finite initial layer thicknesses, and multiple intermetallic layer growth in isothermal or nonisothermal systems.

MODELING

The data from previous work with 63Sn-37Pb solder and 76Au-21Pt-3Pd alloy sheet and thick films (Tables I and II) provided an opportunity to apply the implicit approach discussed above to a "real" system. The experimental data discussed previously indicated that at higher temperatures, only one intermetallic layer approximately $Au_{0.74}Pt_{0.21}Pd_{0.05}Sn_4$ usually forms. Since those data were insufficient to determine which constituent was rate-controlling, the pseudo-constituent $Au_{0.74}Pt_{0.21}Pd_{0.05}$ was chosen as the rate-controlling constituent A for purposes of illustration. The other diffusing species Sn was represented by material B since information on the effects of Pb in the solder was unavailable. With respect to displacement of the solder-IMC interface, this approximation appeared reasonable since previous work done with the 100Sn/Cu and 63Sn-37Pb/Cu systems showed that the Pb-rich phase retreated behind the advancing solder-IMC interface.[6,7] In the porous thick film, it seems probable that a dispersed Pb-rich phase will form. However, information regarding the mechanisms controlling formation of that phase are unavailable, and it was considered more appropriate to use a single approximation for all of the solder, than to "make something up" for the solder in the porous region. In which case, in the reaction zone between materials A and AB_m,

$$\overline{A} + 4B \rightarrow AB_4 \quad (29)$$

and between AB_m and B

$$A + 4\overline{B} \rightarrow AB_4 \quad (30)$$

and intermetallic growth can be described by Eqs. (16) and (18)–(28). Furthermore, the alloy sheet experiments provided data (Table I) for calculating effective diffusion coefficients; some two-dimensional pore space characterization (Table III) was obtained, and data for intermetallic growth in the thick films (Table II) was available for comparison with numerical predictions.

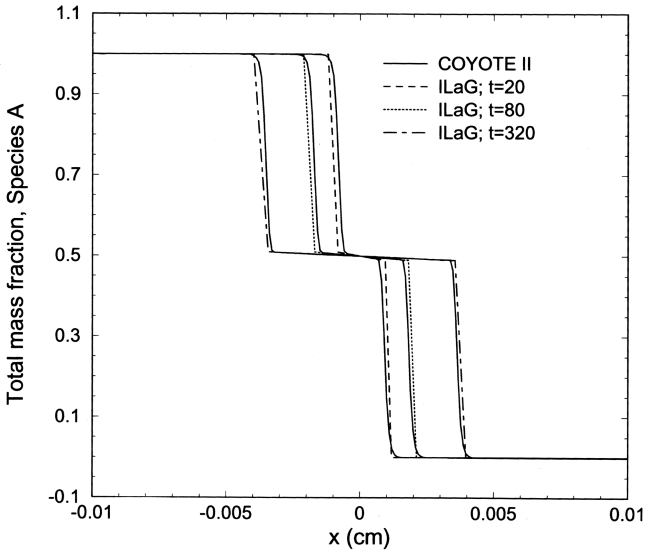

Fig. 6. Comparison of interface displacement calculated explicitly (ILaG) and implicitly (COYOTE II).

Using the data in Table I, effective diffusion coefficients for the pseudo-constituent $Au_{0.74}Pt_{0.21}Pd_{0.05}$ at temperatures 100, 135, and 170°C were calculated as discussed in Appendix B. Because of the large induction period for layer growth at 100°C, evaluation of an Arrhenius expression seemed inappropriate. Values for the other parameters in Eqs. (16) and (18)–(28) are also given in Appendix B.

Numerical Results

Since limited pore space characterization was available, the initial modeling reported below was done using a two-dimensional geometry based on the pore structure shown in Fig. 3 and the characterization data given in Table III. The geometry chosen for the porous thick film and solder consisted of a rectangular region having a width of 50 μm and height of 100 μm. The 2-D representation of the solder and porous thick film is shown in Fig. 7a. The 76Au-21Pt-3Pd thick

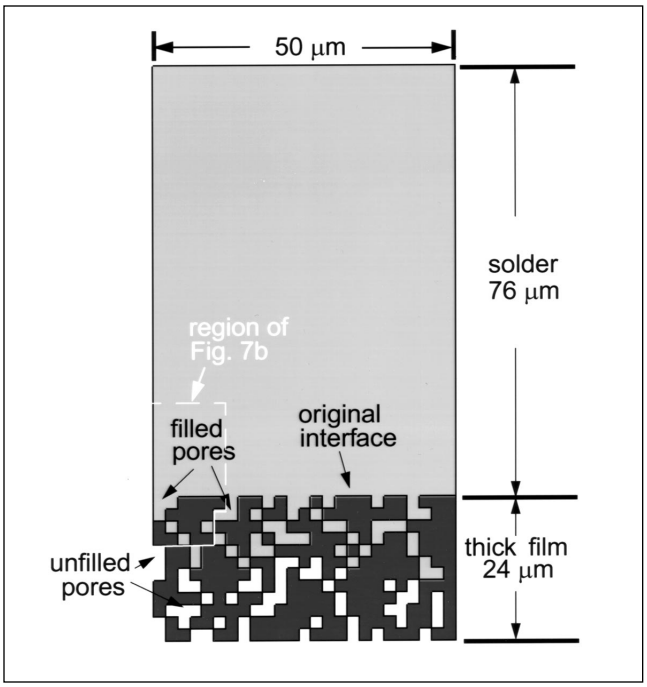

a

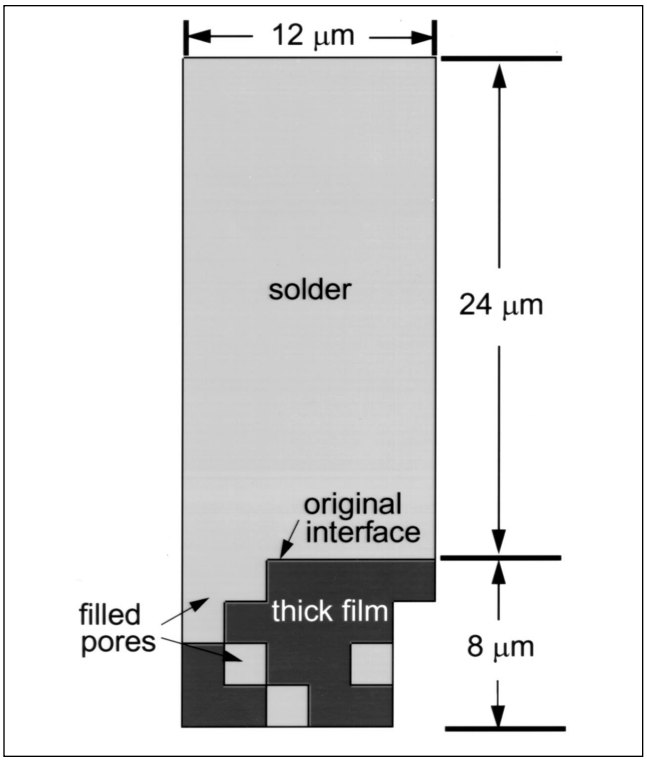

b

Fig. 7. Initial 2-D spatial distribution of solder, porous thick film conductor, solder-filled pores, and voids: (a) Region 50 μm wide by 100 μm high, (b) subregion extending 12 μm to the right of the left boundary in (a), 8 μm below the original interface, and 24 μm above.

film is 24 μm high and is the dark gray region at the bottom of the figure. The solder is 76 μm high and occupies the light gray region above the thick film. The solder-filled pores are shown by the light gray regions within the dark gray thick film, and the unfilled pores are shown in white. The thick film region was divided into 12 rows and 25 columns consisting of square regions having 2 μm sides, which would correspond to a mean area of about 4×10^{-6} mm^2 for each void region. Across each row, the individual squares were randomly selected as 76Au-21Pt-3Pd thick film or void such that the two-dimensional porosity, or pore area fraction, was approximately uniform throughout the thick film region, and the total porosity was about 34 percent.

As mentioned previously, the available experimental data indicated that molten solder initially penetrated the thick film to an average depth of about 8.8 μm below the initial solder-thick film interface. Furthermore, the solder filled about 28 percent of the pore space in the thick film. However in Fig. 7a, the randomly selected void squares in Row 1 (adjacent to the solder) were not directly connected (edge-to-edge) to other void squares below those in Row 2 (the adjacent second row). The squares in Row 2 correspond to a maximum depth of only 4 μm into the thick film. If symmetry were assumed with respect to a third spatial dimension, then the molten solder would penetrate no more than 4 μm into the thick film, and the fraction of the pore space filled with solder would be small. If it were assumed that the distribution of filled and void squares varies in the third dimension, then void squares in rows 3,4,5, etc. could be filled with solder. Therefore, to specify an initial solder distribution in the thick film, it was assumed that connections between pores could occur in a third spatial dimension. Solder was assumed to penetrate the pores to depths ranging from 2 to 14 μm (from Row 1 to Row 7) below the initial interface. The resulting pore area filled by the solder was 16 percent (about 45 percent of the total pore area). Based on that solder distribution, a 2-D finite element mesh was generated with the defined pore geometry, and each square region was identified as either thick film, solder, solder-filled pore, or void. The boundaries of each void were treated as impermeable to a mass flux. The resulting finite element mesh contained about 500,000 nodes. Admittedly, a 2-D simulation done neglecting the third dimension is somewhat artificial. However, in view of the sparse pore space characterization data, a 2-D simulation based on an assumed connection between pores for the purpose specifying the initial solder distribution in the thick film appeared reasonable.

The model described by Eqs. (16) and (18)–(28) was implemented and tested in the multidimensional, massively parallel computer code MPSalsa.[9] Parameter values are given in Appendix B. The value of D_A was 3.1×10^{-11} cm^2/s and represented an average value, as discussed in Appendix B, for earlier times at a temperature of 135°C. Both the geometry and initial conditions used for simulating IMC growth are shown in Fig. 7a. Calculations were carried out on 512 processors of the Intel Teraflop computer due to the problem size and complexity. Even at this level of mesh discretization, about 500,000 nodes, the thin

reaction zone is discernible. The automatic time-stepping algorithm used in the calculations resulted in time steps ranging from about 0.1 to 0.3 days. At each time step, 2 million equations were solved, and the required time was about 40 s. For planning purposes, the time required to calculate IMC growth for t = 30 days would be about 3 h, including overhead for problem distribution and input/output.

Results of the simulation are shown in Figs. 8a, 8b, 8c, and 8d. Gray-scale levels of the IMC $Au_{0.74}Pt_{0.21}Pd_{0.05}Sn_4$ mass fraction, w_{AB_4}, are shown at times of 5, 10, 60, and 90 days. Both the unreacted solder and the 76Au-21Pt-3Pd thick film appear as light gray, and the IMC $Au_{0.74}Pt_{0.21}Pd_{0.05}Sn_4$ appears as dark gray. Figure 8a shows that at 5 days, the IMC has consumed the solder-filled pores, and relative to the initial thick film-solder interface, the IMC-thick film interface has advanced a short distance into the thick film, while the IMC-solder interface has advanced much further into the solder. Only negligible IMC growth has occurred beyond the fill depth of any pore. Figure 8b shows that at ten days, the IMC has grown into the regions between the filled pores, and relative to the initial interface, the IMC has advanced well into the thick film and solder. Figure 8c shows that at 60 days, a very irregular IMC growth pattern has developed in the thick-film region. Finally, Fig. 8d shows that at 90 days, a substantial portion of the thick film has been consumed by IMC formation, and the IMC has advanced to the bottom of the thick film.

To examine IMC growth in more detail, a small region around the initial thick film-solder interface on the left side of Fig. 7a was selected. That region is shown in Fig. 7b and extended 12 μm to the right of the left boundary in Fig. 7a, 8 μm below the original interface, and 24 μm above. Calculations were done similarly to those in Fig. 8 but for times of 0.9, 3.3, 9.3, and 18.5 days. The results are shown in Figs. 9 a, 9b, 9c, and 9d, which further illustrate the complicated geometry of the IMC growth with intersecting and coalescing interfaces. Furthermore, the reaction zone used to implicitly track interface displacement was less than 1 μm thick.

It should be noted that in Fig. 8 and Fig. 9, the IMC layer grows asymmetrically with respect to the original interface. The layer grows more rapidly into the original solder than into the thick film. This asymmetric growth is a direct result of the stoichiometry of

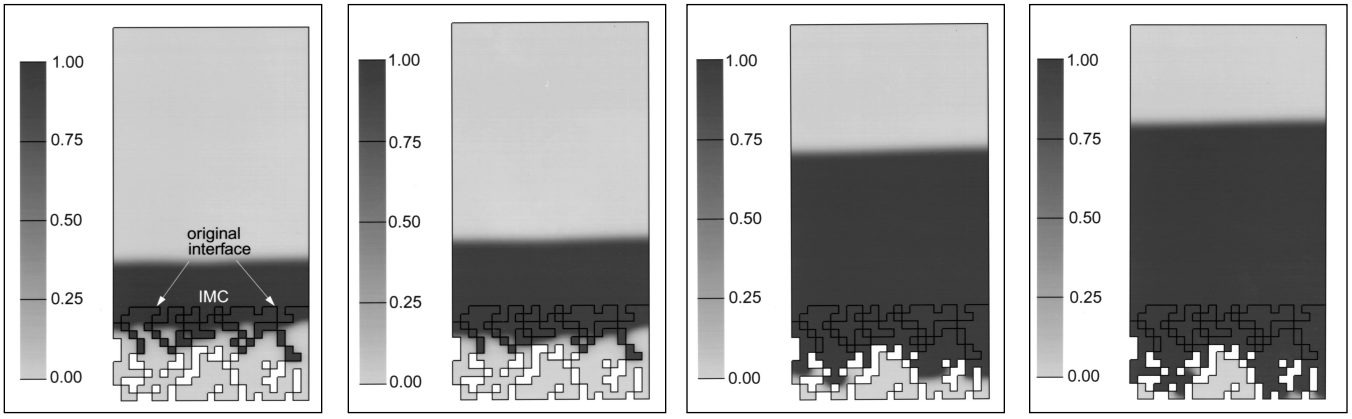

Fig. 8. IMC growth in the geometry shown in Fig. 7a for: (a) 5, (b) 10, (c) 60, and (d) 90 days.

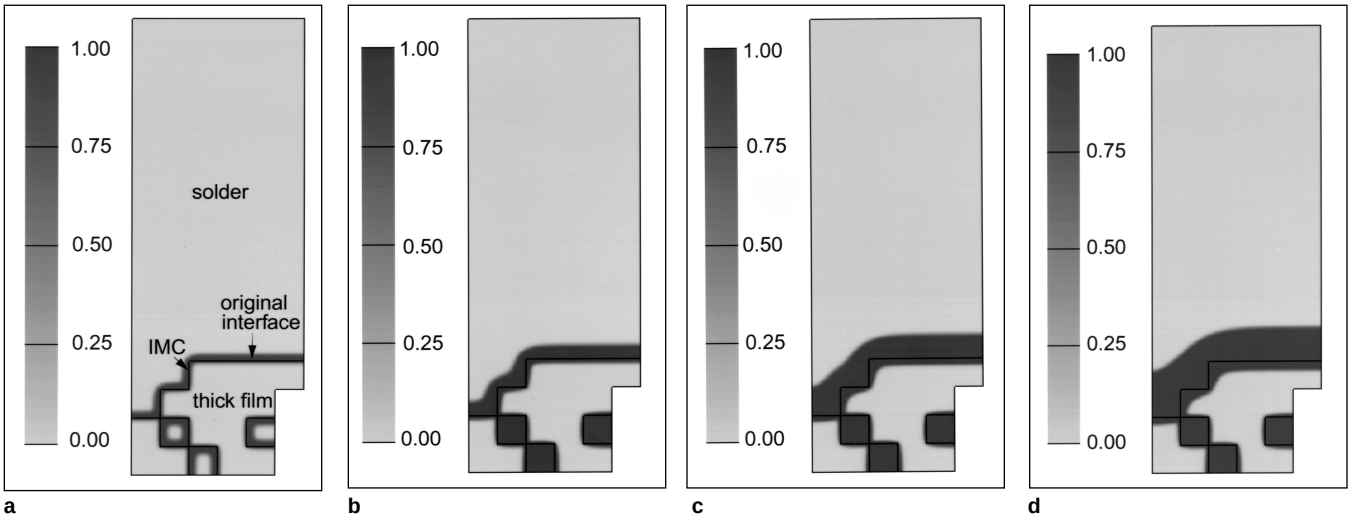

Fig. 9. IMC growth in the geometry shown in Fig. 7b for: (a) 0.9, (b) 3.3, (c) 9.3, and (d) 18.5 days.

the reaction forming $Au_{0.74}Pt_{0.21}Pd_{0.05}Sn_4$. In the case of one-dimensional layer growth involving a nonporous substrate, an analytical expression, which relates IMC growth into the solder and growth into the substrate can be derived from conservation of volume. In particular, for a reaction of the type

$$A+mB \rightarrow AB_m$$

in which the volume change due to reaction can be considered negligible, and the composition of the AB_m product layer is assumed uniform, the following relationship between $\delta_0(t)$, the boundary of the intermetallic AB_m advancing into the substrate A, and $\delta_1(t)$, the boundary advancing into the solder B, is obtained

$$\delta_1(t) = -m\frac{(\rho_A / M_A)}{(\rho_B / M_B)}\delta_0(t) \quad (31)$$

For the parameter values given in Appendix B, the above equation shows that the IMC layer should grow into the solder about six times faster than into the substrate. In Fig. 8, the IMC layer also grows asymmetrically, but less so than predicted for the 1-D case. This difference is due to the porosity in the thick film and the initial percolation of the solder into the pores.

Experimental data for IMC growth relative to the initial interface between thick film and solder were given in Table II. At 135°C, the mean IMC growth between the initial interface and the IMC-solder interface at 273.8 h was 17.0 μm, and growth between the initial and the IMC-thick film interface was 4.5 μm. These growth data can be approximately compared with the predicted IMC growth at 135°C and ten days shown in Fig. 8b, where IMC growth between the initial interface and the IMC-solder interface is about 16 to 18 μm, and growth between the initial and the IMC-thick film interface is 6 to 8 μm. The agreement between experimental and predicted results for IMC growth between the initial interface and the IMC-solder interface is good. The agreement for growth between the initial and IMC-thick film interface is not unreasonable when the approximations and uncertainties associated with representing the pore structure and initial solder distribution in the pores are considered. In fact, these results demonstrate the need for improved characterization of the pore structure and initial solder distribution in the pores so that IMC growth can be effectively modeled in porous thick films.

As a final note, IMC growth can be calculated for a quasi-one-dimensional, nonporous geometry, using Eqs. (37)-(42) in Appendix B. For the same diffusion coefficient and parameter values used in the 2-D simulation discussed above, the IMC growth between the initial interface and the IMC-solder interface at 273.8 h would be 22.2 μm, and IMC growth between the initial and IMC-thick film interface would be 3.6 μm. In this case, growth between the initial and the IMC-solder interfaces is significantly overpredicted, and growth between the initial and the IMC-thick film interfaces is somewhat underpredicted, further illustrating the difficulty in using quasi-one-dimensional analyses to predict IMC growth in thick films. With respect to average interface displacement, some improvement in one-dimensional analyses might be gained by adjusting the diffusion coefficient to reflect a hindered path caused by the pores. However, little would be gained with respect to determining the shape of the interface or the consumption of the material between the pores. Also, adjusting the diffusion coefficient *a priori* could be difficult.

SUMMARY

The integrity of solder joints in (HMC) electronics can be jeopardized by formation of IMC layers, which can have thermal and mechanical properties that are substantially different from the solder and substrate, and which can consume the conductor layer by solid-state reaction. Analytical models predicting IMC growth for a variety of conditions are needed to improve predictions of long-term joint reliability and manufacturing processes. Due to the porosity in thick film conductors, the development of such models is challenging and requires a coupled experimental and computational effort. Experimentally, IMC growth mechanisms and kinetics must be determined, and the pore structure of the thick film must be characterized. Computationally, IMC growth involves a complicated geometry in which the interfaces between solid-state phases grow, intersect, and coalesce. These processes are difficult to model explicitly and are not well predicted by simply applying growth kinetics to a quasi-one-dimensional layer geometry.

This paper summarized initial results from a coupled experimental and computational effort to develop a mathematical model and computer code that will ultimately predict 3-D intermetallic growth in porous substrate-solder systems. The experimental work, reported previously, provided data for parameter evaluation and comparison of experimentally observed and predicted layer growth. The computational work was based on an implicit interface-tracking approach developed for diffusion-reaction analyses in complicated geometries. To illustrate the implicit approach, a model based on implicit interface tracking was implemented in the computer code MPSalsa[9] and used for initial 2-D simulations of the formation and growth of the IMC $Au_{0.74}Pt_{0.21}Pd_{0.05}Sn_4$ between 63Sn-37Pb solder and 76Au-21Pt-3Pd porous thick film substrates. Calculations on a finite element grid of about 500,000 nodes required a massively parallel computer and were performed as a series of calculations on 512 processors of the Intel Teraflop computer. A limited comparison between predicted and experimentally observed IMC growth at 135°C showed good agreement for growth between the initial thick film-solder interface and the IMC-solder interface. However, growth between the initial and IMC-thick film interfaces was overpredicted. For comparison, a quasi-one-dimensional analysis overpredicted IMC growth between the initial and IMC-solder interfaces and underpredicted growth between the initial and IMC-thick film interfaces.

Clearly, IMC growth in the thick film region is dependent on the pore structure of the film and the initial solder distribution in those pores, which also significantly affect the overall film thickness relative to a planar 1-D system.

The model implemented in MPSalsa has clearly demonstrated a capability to address intermetallic growth at sub-micron dimensions in a complicated geometry based on the geometrical characteristics and physical constants from a "real" system. The model can accommodate multiple intersecting and coalescing interfaces and represents a major step toward developing a predictive capability for determining the reliability of HMC solder connects and for developing manufacturing and repair procedures.

Further model development is necessary and requires a continued coupled experimental and computational effort to address several issues. Further experimental work is needed to:

- Determine the behavior of the Pb-rich phase in the solder during IMC growth in the thick-film,
- Determine the mechanisms and kinetics governing IMC growth during the "induction period,"
- Characterize and more accurately describe the pore structure of the thick film in three dimensions, particularly with regard to surface-area-to-volume ratios, and
- Obtain more detailed information on the initial solder distribution in the pores.

Model development should focus on:

- Including the effects of the Pb-rich phase in the solder,
- Expanding the governing equations to include mechanisms controlling IMC growth during the "induction period,"
- Incorporating a more detailed pore structure characterization, and
- Extending calculations to more realistic 3-D geometries.

Additionally, the reaction kinetics portion of the model should be extended to describe the dissolution effects of liquid solder on thick film retention. This issue is particularly pertinent to identifying proper soldering processing parameters for the HMC unit since it is in the soldering phase of the HMC circuit board that the liquid solder can rapidly dissolve the thick film coating. Engineering parameters, such as the actual soldering times used in the assembly process as well as the number of instances that the solder joint can be repaired without complete loss of the thick film conductor, must be accurately predicted in order that reliable products reach the field, whether after initial fabrication or following necessary repair procedures.

Finally, an objective of further experimental and computational work should be to investigate the impact of pore size distribution on the aging of the solder-thick film joints. Thick film materials (e.g., metal powder, binder, or glass frit), as well as the manufacturing processes used to fire the printed ink to the ceramic substrate, can significantly impact the pore size distribution of the post-fired thick film coating and, hence, its survivability under solid-state aging processes.

ACKNOWLEDGMENTS

The authors gratefully acknowledge the technical advice provided by P.A. Sackinger and G.A. Knorovsky of Sandia National Laboratories. Sandia is a multiprogram laboratory operated by Sandia Corporation, a Lockheed Martin Company, for the United States Department of Energy under contract DE-AC04-94AL85000.

REFERENCES

1. N. Shamsunder and E.M. Sparrow, *JHT* 333 (August 1975).
2. A.B. Crowley and J.R. Ockendon, *Intl. J. Heat Mass Transfer* 22, 941 (1979).
3. J.A. Warren and W.J. Boettinger, *Acta Met. et Mater.* 43 (2), 689 (1995).
4. J.S. Langer and R.F. Sekerka, *Acta Met.* 23, 1225 (1975).
5. P.T. Vianco, J.J. Stephens and J.A. Rejent, *IEEE Trans. CPMT*-Part A 20, 470 (1997).
6. K.L. Erickson, P.L. Hopkins and P.T. Vianco, *Analysis of Physiochemical Processes During Solder Aging,* SAND94-0691, (Albuquerque, NM: Sandia National Laboratories, 1994).

7a. P.T. Vianco, K.L. Erickson and P.L. Hopkins, *JEM* 23 (8), 721 (1994).

7b. K.L. Erickson, P.L. Hopkins and P.T. Vianco, *JEM* 23 (8), 729 (1994).

8. P.T. Vianco, P.L. Hopkins, K.L. Erickson, D.R. Frear and R. Davidson, *Design & Reliability of Solders and Solder Interconnections,* (Warrendale, Pa: The Minerals, Metals & Materials Society, 1997), p. 161.
9. J.N. Shadid, et al, *MPSalsa: A Finite Element Computer Program for Reacting Flow Prob lems, Part I - Theoretical Development,* SAND95-2752, (Albuquerque, NM: Sandia National Laboratories, 1996).
10. D.K. Gartling and R.E. Hogan, *COYOTE II - A Finite Element Computer Program for Nonlinear Heat Conduction Problems,* SAND94-1173,(Albuquerque, NM: Sandia National Laboratories, 1994).
11. W. Jost, *Diffusion in Solids, Liquids, Gases,* (New York: Academic Press, 1960).
12. *Lange's Handbook of Chemistry,* 11th Ed., ed. J.A. Dean, (New York: McGraw-Hill, 1973).

APPENDIX A

The implicit formulation described by Eqs. (16) and (18)–(28) was implemented in the well-established finite element code COYOTE II, which solves problems of multidimensional, nonlinear heat conduction, including solid phase chemical reactions.[10] The heat conduction equation solved by COYOTE II is given by

$$\rho C \frac{\partial T}{\partial t} = \frac{\partial}{\partial x_i}\left(k_{ij} \frac{\partial T}{\partial xj} \right) + Q \tag{32}$$

where ρ is the material density; C is the specific heat; k_{ij} is the thermal conductivity tensor; T the temperature, and Q the volumetric heat source. The volumetric heat source includes the energy release due to chemical reactions

$$Q_r = \sum_{j=1}^{J} q_j r_j \tag{33}$$

where q_j is the endothermic or exothermic energy

release, and r_j is the reaction rate for reaction step j. Typically, the reaction rates are functions of the concentration variable for the species. Thus, the species equations solved in conjunction with the thermal problem are given by

$$\frac{dN_i}{dt} = \sum_{j=1}^{J} \nu_{ij} r_j \tag{34}$$

where ν_{ij} are stoiciometric coefficients.

Due to a disparity in time scales between the chemical reactions and thermal diffusion, COYOTE II makes use of an operator splitting method and the use of stiff, ordinary differential equation solvers for the species equations.

To solve equations Eqs. (16) and (18)–(28) using COYOTE II, it was necessary to assume a constant bulk density over a solution time step. This was considered reasonable since the density changes are typically small over time periods and conditions considered. Modifications to COYOTE II were made to allow more general specifications of the coefficients in Eq. (33) and Eq.(34).

APPENDIX B

Equations (2), (4)–(6), and (7)–(8) can be solved analytically,[11] for cases in which: the initial intermetallic layer thickness is negligible; diffusion can be described using Fick's law with constant difffision coefficient; the mass density is essentially constant in each phase, and volume changes due to chemical reaction are negligible. The resulting solution then can be used to obtain values for the effective diffusion coeffficient D_A from experimental data.

Referring to Fig. 4, consider growth of a single intermetallic layer $Au_{0.74}Pt_{0.21}Pd_{0.05}Sn_4$ between the alloy sheet and solder. Let $\delta_0(t)$ denote the interface between the alloy sheet and intermetallic layer, and let $\delta_1(t)$ denote the boundary between the intermetallic and solder. In the region $\delta_0 < x < \delta_1$, the material balance for constituent A is given by Eq. (2)

$$\frac{\partial}{\partial t}(\rho W_A) = \frac{\partial}{\partial x}\left(\rho D_A \frac{\partial w_A}{\partial x}\right) \tag{2}$$

where the subscript 1 has been omitted from terms involving w_A. Initial conditions for Eq. (2) are

$$w_A(x \le 0,\ t = 0) = 1.0$$

and $$w_A(x > 0,\ t = 0) = 0$$

The boundary conditions are

$$w_A(\delta_0^r) = w_{A_1} = \text{a constant}$$

and $$w_A(\delta_1^l) = w_{A_2} = \text{a constant}$$

Also,note that $w_A(x \le \delta_0^l) = 1.0$ and $w_A(x \ge \delta_1^r) = 0$,

The displacements of the interfaces at $\delta_o(t)$ and $\delta_1(t)$ are described by

$$\left(\frac{\rho w_A}{M_A}\bigg|_{\delta_0^l} - \frac{\rho w_A}{M_A}\bigg|_{\delta_0^r}\right)\frac{d\delta_0}{dt} = \frac{\rho D_A}{M_A}\frac{\partial w_A}{\partial x}\bigg|_{\delta_0^r} \tag{35}$$

$$\left(\frac{\rho w_A}{M_A}\bigg|_{\delta_1^l} - \frac{\rho w_A}{M_A}\bigg|_{\delta_1^r}\right)\frac{d\delta_1}{dt} = \frac{\rho D_A}{M_A}\frac{\partial w_A}{\partial x}\bigg|_{\delta_1^l} \tag{36}$$

with the initial conditions $\delta_0(0) = 0 = \delta_1(0)$.

In which case, Eqs. (2), (35), and (36) can be solved analytically to give the following material balance for constituent A in the region $\delta_0 < x < \delta_1$

$$\rho w_A = \rho w_A\big|_{\delta_0^r} + \Gamma\left[\text{erf}\left(\frac{x}{2\sqrt{D_A t}}\right) - \text{erf}(\gamma_0)\right] \tag{37}$$

and displacements of the interfaces at $\delta_0(t)$ and $\delta_1(t)$ are given by

$$\delta_0(t) = 2\gamma_0\sqrt{D_A t} \tag{38}$$

$$\delta_1(t) = 2\gamma_1\sqrt{D_A t} \tag{39}$$

where the constants Γ, γ_0, and γ_1 are given by

$$\Gamma = \frac{\rho w_A\big|_{\delta_0^r} - \rho w_A\big|_{\delta_1^l}}{\left[\text{erf}(\gamma_0) - \text{erf}(\gamma_1)\right]} \tag{40}$$

$$\gamma_0 = \frac{\Gamma \exp(-\gamma_0^2)}{\sqrt{\pi}\left(\rho w_A\big|_{\delta_0^l} - \rho w_A\big|_{\delta_0^r}\right)} \tag{41}$$

$$\gamma_1 = \frac{\Gamma \exp(-\gamma_1^2)}{\sqrt{\pi}\left(\rho w_A\big|_{\delta_1^l} - \rho w_A\big|_{\delta_1^r}\right)} \tag{42}$$

In general, Eqs. (38)–(42) must be solved simultaneously. This can be done using iterative approaches, which are greatly expedited by an additional equation that gives an approximate relationship between $\delta_0(t)$ and $\delta_1(t)$. As previously mentioned, for a reaction of the type

$$A + mB \rightarrow AB_m \tag{43}$$

in which the volume change due to reaction is negligible, and the composition of the AB_m product is assumed uniform, the following additional relationship between $\delta_0(t)$ and $\delta_1(t)$ is obtained from a consideration of conservation of volume

$$\delta_1(t) = -m\frac{(\rho_A / M_A)}{(\rho_B / M_B)}\delta_0(t) \tag{31}$$

Since the stoichiometry of the AB_m product layer does vary slightly with time and position during layer growth, Eq. (31) is only a close approximation when gradients are small and the average stoiciometry of the layer is about AB_m.

Usually, the layer thickness $\Delta(t)$ given by

$$\Delta(t) = \delta_1(t) - \delta_0(t) = 2(\gamma_1 - \gamma_0)\sqrt{D_A t} \tag{44}$$

is determined experimentally, rather than interface displacement or concentration profiles, and Eq. (44) is used to evaluate diffusion coefficients. When the initial layer thickness is finite or unknown, the diffusion coefficient can be estimated from the layer thick-

ness at two times, t_i and t_0, where $t_i > t_0$, by assuming that the concentration profile in the layer at t_0 is approximately given by Eq. (37), so that $\Delta(t_i)$ and $\Delta(t_0)$ are, in principle, given by Eq. (44). Then

$$D_A = \frac{\left[\Delta(t_i)\right]^2 - \left[\Delta(t_0)\right]^2}{4\gamma^2(t_i - t_0)} \quad (45)$$

where $$\gamma = \gamma_1 - \gamma_0 \quad (46)$$

and the interface positions $\delta_i(t)$ and $\delta_0(t)$ are evaluated iteratively using Eqs. (31), (41), and (42).

Because of the long induction periods involved in IMC growth at lower temperatures, the most reasonable temperature on which numerical calculations could be based appeared to be either 135 or 170°C. Since Tables I and II contain more data for IMC growth at 135°C, the calculations were based on this temperature. Although the data for 170°C given in

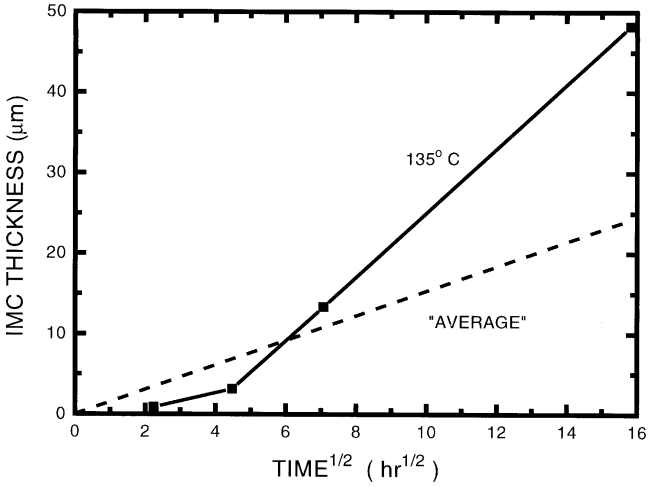

Fig. 10. Early-time IMC growth at 135°C.

Table IV. Data and Values for Effective Diffusion Coefficients for $Au_{0.74}Pt_{0.21}Pd_{0.05}$

Temp. (°C)	Time (h)	Δ(t) (μm)	D_A (cm²/s)	Average D_A (cm²/s)
100	1000 (t_0)	1.05	—	4.2×10^{-13}
	2000	1.69	4.2×10^{-13}	—
135	50 (t_0)	13.34	—	1.5×10^{-10}
	1000	103.4	1.5×10^{-10}	—
170	5 (t_0)	9.81	—	1.5×10^{-9}
	20	40.85	1.4×10^{-9}	—
	1000	344.8	1.6×10^{-9}	—

Table V. Parameter Values

Parameter	Symbol	Value	Comments
Mass density of Au	ρ_{Au}	19.3 (g/cm³)	Reference 12.
Mass density of $Au_{0.76}Pt_{0.21}Pd_{0.03}$	ρ_A	19.3 (g/cm³)	Calculated from densities for Au, Pt, and Pd, assuming negligible volume change due to reaction.
Mass density of $AuSn_4$	ρ_{AuSn_4}	8.9 (g/cm³)	Calculated from densities for Au and Sn, assuming negligible volume change due to reaction. Actual density is 9.2 g/cm³.
Mass density of Sn	ρ_{Sn}	7.3 (g/cm³)	Reference 12.
Mass fractions on left side of $\delta_0(t)$	$w_A(\delta_0^l)$	1.0	Pure constituent.
Mass fractions on right side of $\delta_0(t)$	$w_A(\delta_0^r)$	0.3	Chosen as reasonable value based on Au-Sn phase diagram.
Mass fractions on left side of $\delta_1(t)$	$w_A(\delta_1^l)$	0.28	Chosen as reasonable value based on Au-Sn phase diagram.
Mass fractions on right side of $\delta_1(t)$	$w_A(\delta_1^r)$	0.0	Pure constituent.
Atomic weight of Au	M_A or M_{Au}	118.7 (g/gmole)	Reference 12.
Atomic weight of Sn	M_{Sn}	197.0 (g/gmole)	Reference 12.
	γ_o	–0.032	
	γ_1	0.20	

Table I show a more linear relationship with the $\sqrt{t}$ in Fig. 1, less data is available for IMC growth with both the alloy sheet and porous thick film. Furthermore, 170°C was at the upper extreme in the temperature range studied and may be less representative of actual aging conditions, and for purposes of illustrating the implicit approach for modeling IMC growth in porous thick films, any reasonable value for the diffusion coefficient D_A is sufficient. However, to compare predicted IMC growth with the experimental data given in Table II, the diffusion coefficient should be characteristic of layer growth at earlier times. At 135°C, IMC growth at earlier times varies nonlinearly with the square root of time, as shown in Fig. 10. Since the mechanisms controlling the induction period are not known, the approach taken here was to use a linear relationship with respect to $\sqrt{t}$, shown by the dashed line in Fig. 10, that reasonably represented IMC growth over the time period of interest for comparing predicted IMC growth with the experimental data for the porous thick film.

The diffusion coefficient corresponding to the dashed line in Fig. 10 was calculated from Eq. (44) using the procedure described above. The resulting value was 3.1×10^{-11} cm²/s and was used for all of the numerical calculations. Diffusion coefficients corresponding to longer times in which IMC growth varies linearly with $\sqrt{t}$ were also calculated using Eq. (45) and are summarized in Table IV. In general, the values appear reasonable with respect to published diffusion coefficients for several solid-state systems.[11] Other parameter values used in the numerical calculations and for evaluating diffusion coefficients are given in Table V.